Beyond 300 Gbps Short-Reach Links Using TFLN MZMs With 500 mV_{pp} and Linear Equalization

Essam Berikaa, *Graduate Student Member, IEEE*, Md Samiul Alam, *Member, IEEE*, and David V. Plant, *Fellow, IEEE*

***Abstract*— Driven by the growing data demand and the stringent power constraints on short-reach datacenter interconnects (DCI), this work compares the driver-less (RF driver-free) transmission performance of thin-film lithium niobate (TFLN) Mach-Zehnder modulators (MZM). Two C-band MZMs (18 / 23 mm) fabricated in a commercial foundry are considered. Using the longer MZM with only linear equalization and ∼500 mV_{pp} driving signal, we transmit: (1) 132 Gbaud PAM6 signal (net 309 Gbps) below the 6.7% overhead (OH) hard-decision (HD)-FEC threshold; and (2) 136 Gbaud PAM8 signal (net 342 Gbps) above the 19.02% OH soft-decision (SD)-FEC normalized generalized mutual information (NGMI) threshold of 0.8798 over 500 m of standard single-mode fiber (SSMF). This work demonstrates the feasibility of operating beyond 300 G/lane using TFLN MZMs with CMOS-compatible driving levels.**

***Index Terms*— Datacenter interconnects, thin-film lithium niobate, pulse amplitude modulation.**

I. Introduction

THE data traffic demand is voraciously growing in response to the wide deployment of bandwidth-hungry applications, such as augmented reality applications (Metaverse), cloud-based services, and streaming platforms. Therefore, the capacity of short-reach DCI is stretched to accommodate the growing traffic. Considering short-reach DCI applications under 10 km, intensity modulation direct detection (IMDD) systems are still favored compared with coherent solutions because of IMDD's simpler architecture and lower power requirements. The 800G multi-source agreement (MSA) defined the specifications for the 200 G/lane links [1]; however, there is a persistent need to operate at even higher data rates.

IMDD systems employing simple pulse amplitude modulation (PAM) formats require wide bandwidth electro-optic (EO) modulators to transmit high symbol rate signals. TFLN has emerged as a promising platform for EO modulators because of its high modulation efficiency, negligible optical insertion loss (∼0.3 dB/cm), and low microwave loss [2]; allowing the development of 100 GHz modulators [3], [4]. Yet, TFLN's real promise is operating with CMOS-compatible driving levels and dispensing the power-hungry RF driver circuitry from the transmission system [2], [5], [6], [7]. This is very attractive for DCI applications as it reduces the power consumption considerably. The primary limitation of TFLN modulators is the large footprint; however, novel compact designs are being developed to address this footprint challenge without compromising the EO bandwidth or the modulation efficiency [7], [8].

Several studies considered TFLN in IMDD systems; however, only a few studies operated without RF drivers with sub 1 V_{pp} driving. In [6], the authors demonstrated the driver-less transmission of 70 Gbps on-off keying (OOK) signal under the 6.7% OH HD-FEC BER threshold of 3.8×10^{-3} using 60 mV_{pp} driving swing and a 45 GHz TFLN MZM. The driver-less transmission of 100 Gbaud PAM4 under the KP4-FEC BER threshold of 2.4×10^{-4} is reported using a 45 GHz TFLN MZM [7]. Here, we report the driver-less transmission performance of two C-band TFLN MZMs with varied electrode lengths, 23 mm and 18 mm. We characterize the MZMs and compare their transmission performance, highlighting the design tradeoffs and the characteristics of driver-less operation. Using the long MZM with 500 mV_{pp} driving signal and linear equalization, we report the transmission of 136 Gbaud PAM8 above the 19.02% OH SD-FEC, corresponding to a net rate of 342 Gbps.

II. Experimental Setup and MZM Characterization

Fig. 1 shows the experimental setup and the DSP blocks employed. At the transmitter, PAM4 and PAM8 symbols are generated directly from a random binary sequence, whereas the PAM6 symbols are derived from the standard 32QAM constellation. The generated symbols are then filtered by a raised cosine (RC) pulse shaping filter at 2 samples per symbol (sps), and then resampled to the arbitrary waveform generator (AWG) sampling rate (256 GSa/s). We pre-compensate the frequency response of the AWG and a 10 cm RF cable (1.85 mm connectors) up to 75 GHz using the digital pre-emphasis filter depicted in the inset of Fig. 1. The 10 dB point is around 70 GHz. We are not employing a RF driver after the AWG; thus, clipping the signal is essential to limit its peak-to-average power ratio (PAPR). Signal clipping reduces the PAPR and subsequently increases the root mean square (RMS) of the driving signal at the expense of inducing some nonlinearity and distortion in the generated signal. The clipped signal is loaded to the AWG running at 256 GSa/s, which drives the TFLN MZM directly through a 67 GHz GSG probe. Optically, the

Manuscript received 8 August 2022; revised 3 November 2022; accepted 2 December 2022. Date of publication 6 December 2022; date of current version 14 December 2022. This work was supported by the Fonds de Recherche du Quebec—Nature et Technologies under Grant 320758. *(Corresponding author: Essam Berikaa.)*

The authors are with the Photonic Systems Group, Department of Electrical and Computer Engineering, McGill University, Montreal, QC H3A 0E9, Canada (e-mail: essam.berikaa@mail.mcgill.ca; md.samiul.alam@mail.mcgill.ca; david.plant@mcgill.ca).

Color versions of one or more figures in this letter are available at https://doi.org/10.1109/LPT.2022.3227085.

Digital Object Identifier 10.1109/LPT.2022.3227085

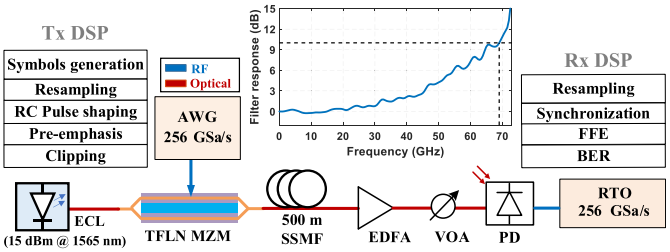

Fig. 1. (a) The experimental setup and DSP blocks employed at the transmitter (Tx) and receiver (Rx). The inset shows the pre-compensation filter response.

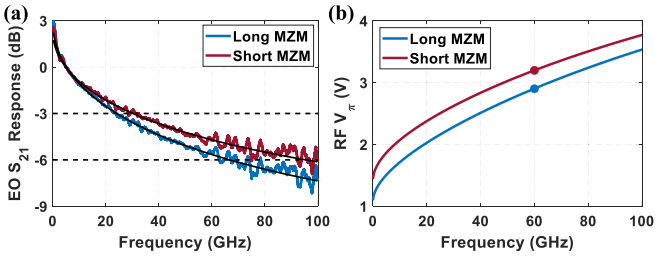

Fig. 2. (a) The EO frequency response normalized to 5 GHz. (b) The measured and extrapolated RF V_π of the long and short TFLN MZMs.

TABLE I

SUMMARY OF NET BITRATE ACHIEVED AFTER 500 M TRANSMISSION USING ~500 mV_{PP} DRIVING SIGNALS AND FFE

FEC	Short TFLN MZM		Long TFLN MZM	
	Modulation format	Net rate (Gbps)	Modulation format	Net rate (Gbps)
KP4-FEC	105 Gbaud PAM6	250	108 Gbaud PAM6	256
	128 Gbaud PAM4	242	132 Gbaud PAM4	250
HD-FEC	128 Gbaud PAM6	300	132 Gbaud PAM6	309
	144 Gbaud PAM4	270	144 Gbaud PAM4	270
SD-FEC	132 Gbaud PAM8	332	136 Gbaud PAM8	342

TFLN MZM is fed by a 15 dBm tunable external cavity laser (ECL) and is connected via vertical grating couplers (VGC) that have 10 dB back-to-back coupling loss. The output of the MZM is transmitted over 500 m of SSMF, corresponding to ~8-9 ps/nm dispersion. This is equivalent to the dispersion induced by 10 km O-band transmission for the edge channels in the coarse wavelength division multiplexing (CWDM) grid. We needed to boost the optical power (to 7 dBm) before the receiver using an EDFA to compensate for the VGCs loss since we employed a conventional 70 GHz PIN photodiode (PD, 0.63 A/W) without a trans-impedance amplifier (TIA). Practically, the TFLN MZM will be connected via edge couplers (1.5 dB/facet), and a high bandwidth PIN PD with TIA can improve the receiver sensitivity; dispensing the need for optical amplification. The variable optical attenuator (VOA) is added for sweeping the received optical power (ROP). The PD output is captured by the 256 GSa/s real-time oscilloscope (RTO) and processed offline. At the receiver, we first resample the received signal to 2 sps and process it with a 71 tap T/2 spaced linear feed-forward equalizer (FFE), unless mentioned otherwise. Finally, the equalized signals are down-sampled to 1 sps for BER/ NGMI calculations.

Operating without an RF driver has several implications on the system performance as follows: (1) the driving signal swing is smaller, which ensures within the linear part of the MZM transfer function and alleviates the nonlinearity concerns at the expense of a lower optical extinction ratio after modulation; (2) it yields higher signal-to-noise ratio of the driving RF signal; and (3) it improves the system bandwidth as the RF driver induces some drop at 70 GHz. Thus, only linear signal processing is considered in this work. Employing nonlinear equalizers improves the performance marginally, which does not justify the added complexity. Moreover, dispensing the RF driver reduces the overall system cost, power consumption, and packaging requirements; however, it might lead to a manageable penalty in the transmission performance, as discussed in the next section.

This work compares the driver-less transmission performance of two TFLN MZMs fabricated on the same run at an accessible foundry. The MZMs have the same structure and differ only in the coplanar waveguide electrode lengths: 23 mm long MZM and 18 mm short MZM. The MZMs come with nearly 50 Ω on-chip termination and are biased with a thermal phase shifter. Fig. 2(a) shows the measured frequency response of both MZMs. The long MZM has a 24 (66) GHz 3-(6-) dB bandwidth, while the short MZM has 30 (95) GHz 3-(6-) dB bandwidth. Since we pre-compensate the AWG frequency response at the transmitter, the receiver DSP needs to equalize the frequency response of the MZM and PD only. Thus, the 6-dB bandwidth is more relevant in this case. Despite the difference in their 6-dB bandwidths, the difference at 70 GHz is only 1 dB owing to the slow roll-off response of TFLN modulators [2]. Fig. 2(b) shows the RF V_π of both MZMs. The RF V_π is measured by biasing the MZM at maximum transmission and monitoring the output average optical power as a function of the amplitude (V_{pp}) of a 60 GHz single-tone signal. The V_π at 60 GHz is extracted from the normalized optical power versus the V_{pp}/V_π relationship, which follows a Bessel function formula. Then, we extrapolate the RF V_π from DC to 100 GHz using the MZMs' measured frequency response. The low-MHz V_π of the long and short MZMs are 1.25 V and 1.5 V, which increase to 3 V and 3.3 V at 70 GHz, respectively. The measured DC extinction ratio of the long MZM is 25 dB compared to 35 dB for the short MZM. Our system is limited by the driving signal swing and the bandwidth of the AWG; therefore, the difference in their V_π is more impactful than the difference in the bandwidth and extinction ratio.

III. DRIVER-LESS TRANSMISSION RESULTS

Fig. 3 presents the transmission performance achieved using the long and short MZMs. The BER versus symbol rate of PAM4 and PAM6 signals after 500 m transmission is given in Fig. 3 (a) with the summary in Table I. The long MZM outperforms the short MZM throughout the considered symbol rates (100 to 150 Gbaud). Using the long MZM, we transmit 108 and 132 Gbaud PAM6 signals under the KP4-FEC threshold and the 3.8×10^{-3} HD-FEC BER threshold, respectively, which correspond to a net rate of 256 and 309 Gbps. Besides, we transmit 105 and 128 Gbaud PAM6 signals using the short MZM below the KP4-FEC and HD-FEC BER thresholds, corresponding to net rates of 250 and 300 Gbps.

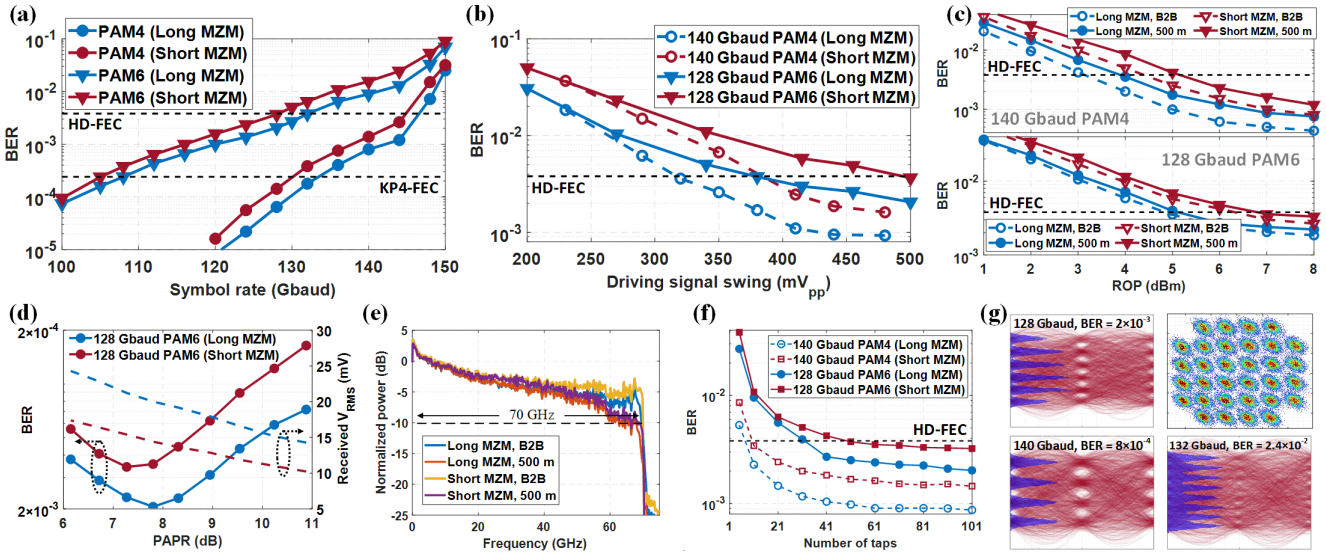

Fig. 3. (a) The BER versus the symbol rate (ROP = 7 dBm). (b) The BER sensitivity to the driving voltage swing (ROP = 7 dBm). (c) The BER versus ROP at 140 Gbaud PAM4 and 128 Gbaud PAM6 in B2B and after 500 m transmission. (d) The BER versus the PAPR of 128 Gbaud PAM6, and the corresponding received signal RMS on the right y axis. (e) The received RF spectra of 140 Gbaud PAM4 signals. (f) The BER sensitivity to the number of FFE taps. (g) The eye diagrams after the FFE for 140 Gbaud PAM4, 128 Gbaud PAM6 (constellation diagram), and 132 Gbaud PAM8 after 500 m transmission using the long MZM.

Fig. 3(b) shows the BER dependency on the driving signal swing for 140 Gbaud PAM4 and 128 Gbaud PAM6 signals using both long and short MZMs. Using the long MZM, we transmit 140 Gbaud PAM4 using an exceptionally low swing of 325 mV_{pp} under the HD-FEC BER threshold, while a minimum of 400 mV_{pp} is required for transmitting 128 Gbaud PAM6. The short MZM requires a higher swing to achieve the same BER because of its higher V_π. The smaller driving signal swing implies reducing the power consumption, which is extremely important for short-reach DCI solutions. CMOS can fulfill these low swing requirements, which supports TFLN as a platform for next-generation EO modulators.

The BER sensitivity to the ROP both in back-to-back (B2B) and after 500 m transmission is given in Fig. 3(c). Compared to the long MZM, the short MZM exhibits a ∼1 dB ROP penalty. This ROP penalty arises from the inherent difference in the modulation efficiency of the long and short MZM. Going from B2B to 500 m, the transmission penalty is more pronounced for the 140 Gbaud PAM4 cases because of the stronger chromatic dispersion (CD)-induced power fading. Fig. 3(e) shows the received RF spectra of 140 Gbaud PAM4 signals. Compared to the short MZM, the long MZM has an extra 1 dB drop at 70 GHz because of the intrinsic difference in their EO response. However, the ∼5.5 dB drop at 70 GHz after transmission stems from the CD-induced power fading.

The swing limitations in our system dictate optimizing the PAPR to compromise the swing and nonlinearity constraints. Here we control the PAPR by clipping the digital signal before loading it to the AWG. Fig. 3(d) shows the BER performance of 128 Gbaud PAM6 signals after 500 m transmission and the received signal RMS as a function of the PAPR of the digital signal loaded to the AWG. The clipping improves the signal swing, leading to an increase in extinction ratio. However, strong clipping distorts the signal and causes overall BER degradation. For our system, the optimum PAPR for 128 Gbaud PAM6 signal is ∼7.8 dB and 7.25 dB for the long and short MZMs, respectively. Besides, the received signal RMS for the long MZM is considerably higher than that for the short MZM owing to the higher modulation depth in the former case.

The BER sensitivity to the number of FFE taps is given in Fig. 3 (f). Only 11 filter taps are needed for transmitting 140 Gbaud PAM4 under the HD-FEC threshold, and 51 taps are required to reach the BER floor for both MZMs as the difference in the received frequency response is marginal (∼1 dB). Fig. 3 (g) shows the generated eye diagrams of the equalized signals at different symbol rates and PAM formats after 500 m transmission using the long MZM. Interestingly, the generated constellation from the 128 Gbaud PAM6 signal shows elliptical noise distribution, highlighting the impact of the FFE-enhanced in-band noise [9]. Employing equalization-enhanced noise reduction algorithms or joint feed-forward and decision-feedback equalization will improve the transmission performance further.

To determine the attainable transmission rates, we considered PAM8 transmission adopting SD-FEC with an NGMI threshold of 0.8798 (code rate: 0.84) [10]. Fig. 4(a) shows the calculated NGMI after 500 m transmission. Using only linear equalization and ∼500 mV_{pp} driving signal, we transmit 136 Gbaud PAM8 using the long MZM well above the NGMI threshold, corresponding to a net rate of 342 Gbps. The short MZM enabled transmitting 132 Gbaud PAM8, which corresponds to a net rate of 332 Gbps. Fig. 4(b) shows the ROP performance of 132 Gbaud PAM8 for both MZMs. Here, the short MZM exhibits a higher ROP penalty of ∼2 dB, which stems from the higher number of levels of PAM8 and the higher sensitivity to the received signal swing. Fig. 4(c) shows the NGMI sensitivity to the driving signal swing, the difference in performance between the long and short MZMs

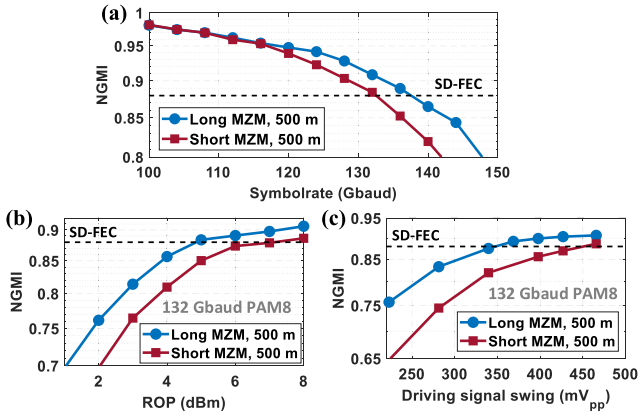

Fig. 4. (a) NGMI versus symbol rate for PAM8 signals. (b) NGMI versus ROP and (c) NGMI sensitivity to the driving swing of 132 Gbaud PAM8.

is more pronounced in the PAM8 case. We transmit 132 Gbaud PAM8 signal over 500 m above the SD-FEC NGMI threshold with only 375 mV_{pp} using the long MZM.

The differences in transmission performance between the long and short MZMs are mainly because of the difference in their V_π, given their high bandwidth and the AWG bandwidth limitations. Although the short MZM has higher bandwidth and extinction ratio, its higher V_π results in lower modulation depth, smaller signal swing at the receiver, and slightly worse overall performance. Thus, reducing the MZM V_π via increasing its length is advantageous; however, the footprint of short-reach pluggable modules is the limiting factor. The sensitivity of the performance to the driving swing scales with the PAM order because of the higher number of levels and the modest optical extinction ratio after modulation; thus, PAM4 is more suitable for such driver-less systems.

Several reports showed the IMDD transmission of over 300 Gbps with transmitters employing RF drivers [11], [12], [13], [14], [15], [16], [17], [18], [19]; yet, this is the first demonstration of net 300 Gbps transmission in a driver-less scenario. Our results indicate the promise of 300 Gbps short-reach DCI links based on TFLN MZMs with reduced DSP complexity and low driving voltage requirements (below 500 mV_{pp}). In [13], we report the transmission results obtained using the short MZM and employing RF driver, where we transmitted 132 Gbaud PAM6 signal over 500 m below the HD-FEC BER threshold, and 140 Gbaud PAM8 signal above the SD-FEC NGMI threshold using non-linear processing at the transmitter and receiver, which respectively correspond to net rates of 309 and 352 Gbps. Those results are on par with what is achieved in this work using the long MZM without the RF driver and only linear equalization. This suggests that the driving signal swing improvement because of the RF driver is counteracted by the added noise, which degrades the RF signal quality and results in marginal improvement.

IV. Conclusion

This work presents an experimental comparative study between two C-band TFLN MZMs with 23 and 18 mm electrodes. Owing to the MZMs' low V_π, the transmission performance is evaluated in a driver-less scenario with a driving signal swing of ∼500 mV_{pp}. Using only linear equalization, we transmit 132 Gbaud PAM4 signal under the 5.2% OH KP4-FEC threshold, 132 Gbaud PAM6 signal below the 6.7% OH HD-FEC BER threshold, and 136 Gbaud PAM8 above the 19.02% OH SD-FEC NGMI threshold, which respectively represent net rates of 250, 309, and 342 Gbps. Our analysis indicates that the MZM V_π is the defining parameter for its driver-less performance and that employing an RF driver improves the performance marginally.

Acknowledgment

The authors would like to thank HyperLight for their support on the TFLN modulator.

References

[1] *800G Pluggable MSA*. Accessed: Aug. 1, 2022. [Online]. Available: https://www.800gmsa.com/
[2] D. Zhu et al., "Integrated photonics on thin-film lithium niobate," *Adv. Opt. Photon.*, vol. 13, no. 2, pp. 242–352, 2021.
[3] P. O. Weigel et al., "Bonded thin film lithium niobate modulator on a silicon photonics platform exceeding 100 GHz 3-dB electrical modulation bandwidth," *Opt. Exp.*, vol. 26, no. 18, pp. 23728–23739, 2018.
[4] F. A. Juneghani et al., "Demonstration of non-symmetric thin-film lithium niobate modulator with a 3-dB bandwidth beyond 100 GHz," in *Proc. CLEO, Sci. Innov.*, 2022. p. SF4G.1.
[5] M. Xu et al., "Thin-film lithium niobate DP-IQ modulator for driverless 130 Gbaud 64 QAM transmission," in *Proc. Opt. Fiber Commun. Conf.*, 2022, p. Th1J.2.
[6] C. Wang et al., "Integrated lithium niobate electro-optic modulators operating at CMOS-compatible voltages," *Nature*, vol. 562, no. 7725, pp. 101–104, 2018.
[7] G. Chen et al., "Compact 100 GBaud driverless thin-film lithium niobate modulator on a silicon substrate," *Opt. Exp.*, vol. 30, no. 14, pp. 25308–25317, 2022.
[8] X. Liu et al., "A highly compact thin-film lithium niobate modulator with low half-wave voltage," in *Proc. Opt. Fiber Commun. Conf.*, 2022, p. Th1J.6.
[9] E. Berikaa, M. S. Alam, M. Jacques, X. Li, P.-C. Koh, and D. V. Plant, "2D constellation distortion for subduing equalization noise in bandwidth-limited IMDD systems," *IEEE Photon. Technol. Lett.*, vol. 34, no. 5, pp. 267–270, Mar. 1, 2022.
[10] J. Cho and L. Schmalen, "Construction of protographs for large-girth structured LDPC convolutional codes," in *Proc. IEEE Int. Conf. Commun. (ICC)*, Jun. 2015, pp. 4412–4417.
[11] D. Che and X. Chen, "Higher-order modulation vs faster-than-Nyquist PAM-4 for datacenter IM-DD optics: An AIR comparison under practical bandwidth limits," *J. Lightw. Technol.*, vol. 40, no. 10, pp. 3347–3357, May 15, 2022.
[12] H. Yamazaki et al., "Net-400-Gbps PS-PAM transmission using integrated AMUX-MZM," *Opt. Exp.*, vol. 27, no. 18, pp. 25544–25550, 2019.
[13] M. S. Alam, E. Berikaa, and D. V. Plant, "Net 350 Gbps/λ IMDD transmission enabled by high bandwidth thin-film lithium niobate MZM," *IEEE Photon. Technol. Lett.*, vol. 34, no. 19, pp. 1003–1006, Oct. 1, 2022.
[14] X. Chen et al., "Single-wavelength and single-photodiode 700 Gb/s entropy-loaded PS-256-QAM and 200-GBaud PS-PAM-16 transmission over 10-km SMF," in *Proc. Eur. Conf. Opt. Commun. (ECOC)*, 2020, pp. 1–4.
[15] M. Eppenberger et al., "Plasmonic racetrack modulator transmitting 220 Gbit/s OOK and 408 Gbit/s 8PAM," in *Proc. Eur. Conf. Opt. Commun. (ECOC)*, 2021, pp. 1–4.
[16] M. S. Alam, X. Li, M. Jacques, E. Berikaa, P.-C. Koh, and D. V. Plant, "Net 300 Gbps/λ transmission over 2 km of SMF with a silicon photonic mach–zehnder modulator," *IEEE Photon. Technol. Lett.*, vol. 33, no. 24, pp. 1391–1394, Dec. 15, 2021.
[17] M. S. B. Hossain et al., "402 Gb/s PAM-8 IM/DD O-band EML transmission," in *Proc. Eur. Conf. Opt. Commun. (ECOC)*, 2021, pp. 1–4.
[18] Q. Hu et al., "Plasmonic-MZM-based short-reach transmission up to 10 km supporting >304 GBd polybinary or 432 Gbit/s PAM-8 signaling," in *Proc. Eur. Conf. Opt. Commun. (ECOC)*, 2021, pp. 1–4.
[19] J. Zhang et al., "Nonlinearity-aware PS-PAM-16 transmission for C-band net-300-Gbit/s/λ short-reach optical interconnects with a single DAC," *Opt. Lett.*, vol. 47, no. 12, pp. 3035–3038, 2022.